Research in Astron. Astrophys. **2013** Vol. **13** No. **5**, 615–628
http://www.raa-journal.org *http://www.iop.org/journals/raa*

*R*esearch in
*A*stronomy and
*A*strophysics

Evaluation of a scientific CMOS camera for astronomical observations

Peng Qiu[1,2,3,4], Yong-Na Mao[2,3,4], Xiao-Meng Lu[2,3,4], E Xiang[2,3,4] and Xiao-Jun Jiang[2,4]

[1] Xinjiang Astronomical Observatories, Chinese Academy of Sciences, Urumqi 830011, China; *pqiu@bao.ac.cn*
[2] National Astronomical Observatories, Chinese Academy of Sciences, Beijing 100012, China
[3] University of Chinese Academy of Sciences, Beijing 100049, China
[4] Key Laboratory of Optical Astronomy, National Astronomical Observatories, Chinese Academy of Sciences, Beijing 100012, China

Received 2012 April 18; accepted 2012 November 9

Abstract We evaluate the performance of the first generation scientific CMOS (sCMOS) camera used for astronomical observations. The sCMOS camera was attached to a 25 cm telescope at Xinglong Observatory, in order to estimate its photometric capabilities. We further compared the capabilities of the sCMOS camera with that of full-frame and electron multiplying CCD cameras in laboratory tests and observations. The results indicate the sCMOS camera is capable of performing photometry of bright sources, especially when high spatial resolution or temporal resolution is desired.

Key words: instrumentation: detectors: sCMOS, CCD

1 INTRODUCTION

Both CMOS cameras and CCD cameras convert incident photons into electrons in accordance with the photoelectric effect. However, their different pixel structures lead to differences in characteristics of their performance. Conventional CMOS cameras are not widely applied to astronomical observations because of their higher readout noise (RN), pixel nonuniformity, lower quantum efficiency (QE) and fill factor as compared with CCD cameras. However, due to the rapid development of CMOS technology in the past decade, the CMOS camera has shown its advantages in observations with high spatial resolution and rapid frame rate (Hoffman et al. 2005).

An application of an IBIS5 CMOS camera to astronomical observation indicated that it performed well in applications where a large dynamic range is required. However, its high dark current and pixel-to-pixel nonuniformity still need to be improved (Shang & Song 2006). We purchased the first generation scientific CMOS (sCMOS) camera from Andor Technology PLC; its 5.5 megapixel sensor offers high spatial and temporal resolution with low RN. The sCMOS camera is mounted on a 25 cm f/3.6 Newtonian reflector at Xinglong Observatory, National Astronomical Observatories, Chinese Academy of Science. Compared to the IBIS5 CMOS camera, the sCMOS camera has the following advantages: four times larger chip size, higher QE, higher fill factor (more than 90%), higher frame rate, higher dynamic range and lower RN. It is important to evaluate if the sCMOS is suitable for more applications in astronomical observations. For a better evaluation, a full-frame CCD (FFCCD) and an electron multiplying CCD (EMCCD) are used to make comparisons with the sCMOS (Waltham 2010; Janesick et al. 2002).

This paper is organized as follows. We calculate the theoretical dynamic range and photometric accuracy of the sCMOS, FFCCD and EMCCD in Section 2. In Section 3 we present the evaluation, as well as the results from laboratory tests and observations of real stars. The conclusion is shown in Section 4.

2 SPECIFICATIONS OF THE SCMOS, FFCCD AND EMCCD

FFCCD and EMCCD cameras are frequently used in professional observations. At Xinglong Observatory, FFCCD cameras are equipped on larger telescopes (i.e. the 4 m Guo Shou Jing Telescope and 2.16 m telescope) for spectroscopy and smaller telescopes for photometry. An EMCCD camera is equipped on a 1 m telescope for time-series photometry. The FFCCD (VersArray 1300B by Princeton Instruments) and EMCCD (DU-888E by Andor Technology) are chosen to compare with the sCMOS (DC-152Q-FI by Andor Technology) for better investigation of its application for astronomical observations.

2.1 Specifications

Specifications of the sCMOS, FFCCD and EMCCD that we tested are shown in Figure 1 and Table 1[1]. The FFCCD has the largest imaging area of 26.8 mm$\times$26.0 mm and highest pixel well depth for an active area of 210 000 e^-. The EMCCD has an ultra-low dark current of 0.001 e^- pixel^{-1} s^{-1} at –75°C and highest peak QE of about 97% at 570nm. Compared with the FFCCD and EMCCD, the sCMOS has more active pixels, smaller pixel size, lower RN and higher frame rate, but lower QE and well depth.

Fill factor is the percentage of the light-sensitive portion of the pixel. A fill factor which cannot reach 100% will affect the photometric accuracy, because the camera cannot collect photons from the targets if they reach the portions of the pixels that are not light sensitive. Compared with scientific grade CCD cameras, the fill factors of CMOS cameras cannot reach 100% due to the different structures of pixels (Fig. 2). The fill factors of conventional CMOS cameras range from 30% to 40%, which is one of the reasons why they are not widely applied to astronomical observations. For the sCMOS we tested, the fill factor is more than 90% (email communication from Andor Technology, Beijing Representative Office). A fill factor has different effects on photometric accuracies. When oversampling, the target is distributed over a number of pixels, in which the portions that are not light sensitive are small parts of the star image, thus the photometric accuracy is hardly affected in this case. However, when undersampling, the target is concentrated on fewer pixels, so the effect of the portions that are not light sensitive would be noticeable, and the photometric accuracy may be greatly affected in this case.

2.2 Theoretical Dynamic Range and Photometric Accuracy

The sCMOS has a dual-amplifier architecture, in which data can be sampled simultaneously by both high gain and low gain amplifiers. The architecture is designed to simultaneously minimize RN and maximize dynamic range. The sensor has four individual 11-bit gain settings (PAG1, PAG2, PAG3, PAG4) and one dual-amplifier 16-bit setting (Dual: PAG1 and PAG4) (sCMOS technical notes 2010). The detailed specifications of the three cameras are listed in Appendix A. The parameters of the settings we used during the evaluation are listed in Table 2.

[1] Data describing the sCMOS, FFCCD and EMCCD in Figure 1 and Table 1 are from the manufacturers' data sheets of Andor Technology sCMOS DC-152Q-FI, Princeton Instruments VersArray: 1300B, and Andor Technology *iXon*$^{\mathrm{EM}}$ DU-888E, respectively.

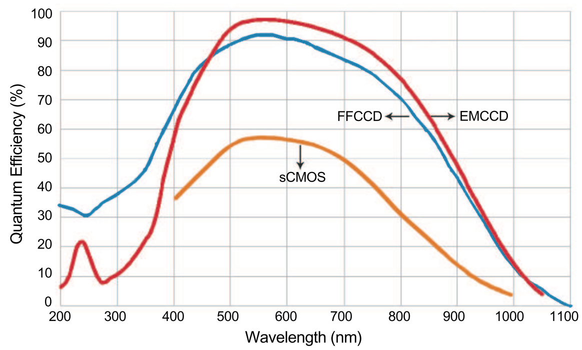

Fig. 1 Quantum Efficiency Curves of the sCMOS, FFCCD and EMCCD that we tested.

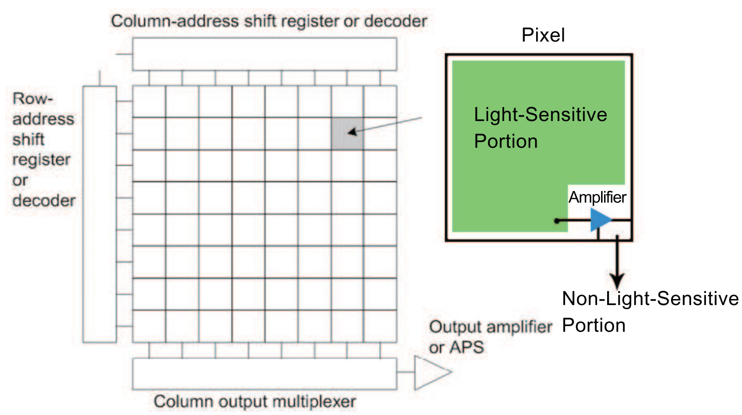

Fig. 2 Simple architecture of a CMOS array. The CMOS has an independent amplifier in each pixel, which converts the integrated charge into voltage. Because the amplifier shares the pixel area, the fill factor could not reach 100%.

The dynamic range of a CCD is defined as the ratio of the full well depth of one pixel to the RN of the detector (Howell 2006). However, the dynamic range of an EMCCD with application of EM gain is defined as the ratio of the full well capacity of one pixel to the detection limit (Andor Technology 2009). We calculate the theoretical dynamic range of the sCMOS, FFCCD and EMCCD, which is shown in Table 3.

We calculate the signal-to-noise (S/N) value obtained for a given camera system and integration time based on Equation (1) (Howell 2006), and our calculations of photometric accuracy are also based on this equation.

The source S/N equation is

$$\mathrm{S/N} = \frac{R_* \times t}{\left(R_* \times t + R_{\mathrm{sky}} \times t \times n_{\mathrm{pix}} + \mathrm{RN}^2 \times n_{\mathrm{pix}} + (\mathrm{Gain}/2)^2 \times n_{\mathrm{pix}} + D \times n_{\mathrm{pix}} \times t\right)^{1/2}} \tag{1}$$

and

$$R_* = \mathrm{QE} \times R_{\mathrm{obj}} \times 10^{-0.4 \times k' \times \mathrm{airmass}}. \tag{2}$$

Table 1 Factory Specifications of the sCMOS, FFCCD and EMCCD

Camera	sCMOS DC-152Q-FI	FFCCD VersArray 1300B	EMCCD DU-888E
Active Pixels	2560×2160	1340×1300	1024×1024
Pixel Size (W×H; μm)	6.5×6.5	20×20	13×13
Image Area (mm)	16.6×14.0	26.8×26.0	13.3×13.3
Well Depth (e^-, typical)	30 000	210 000	88 000[1] ; 730 000[2]
Frame Rate (frame s^{-1})	30[3]	0.56	8.9
Readout Noise (e^-, typical)	1@100 MHz 1.4@280 MHz	2.8@100 kHz 8@1 MHz	7.7@1 MHz 45@10 MHz
Dark Current (e^- pixel^{-1} s^{-1})	0.03@–40°C	0.3@–40°C	0.001@–75°C
Fill Factor	>90%	100%	100%
Peak QE (typical)	57% @570 nm	93% @570 nm	97% @570 nm

Notes: [1] The well depth of the active area of a pixel. [2] The well depth of the gain register of a pixel. The gain register has a linear response up to 400 000 e^- and a full well depth of 730 000 e^- at maximum (Andor Technology *iXon*$^{\mathrm{EM}}$ DU-888E 2009). [3] With the cameralink base in Rolling Shutter readout mode (Andor Technology sCMOS DC-152Q-FI 2010).

Table 2 The Parameters of the Settings Used in Evaluation

Camera	System Readout Rate	Preamp setting	Gain	RN	Well Depth
sCMOS	280MHz 16-bit	Dual	0.66	1.14	30 000
FFCCD	2.0MHz 16-bit	Low	4.17	7.33	210 000
EMCCD	10MHz 14-bit	2.4	21.13	50.29	88 000; 730 000

Table 3 Dynamic Range of the Cameras in Different Settings

Camera	System Readout Rate	Preamp setting	Gain	RN	Dynamic Range
sCMOS	280MHz 16-bit	Dual	0.66	1.14	26 316:1
FFCCD	2.0MHz 16-bit	Low	4.17	7.33	28 649:1
EMCCD	10MHz 14-bit	2.4	21.13	50.29	1750:1[1]; 6884:1[2]

Notes: [1] EM gain is turned off. [2] EM gain is set at 4.

The above S/N equation is effective for a given CCD measurement of a source. However, it is unsuitable for EMCCD with application of EM gain because the S/N value of an EMCCD is affected by application of a gain register. The gain register can effectively amplify the signal (especially for faint sources); in other words, it can eliminate the RN contribution to the detection limit. However, a statistical variation is generated, which is quantified at a value of $\sqrt{2}$ called the "Noise Factor'' (Andor Technology 2009). Thanks to thermoelectric (TE) cooling (at least –75°C), the contribution of dark current (for a short exposure time) can be ignored.

In this paper, the S/N equation for EMCCD with application of EM gain is simplified as

$$\mathrm{S/N} = \frac{R_* \times t \times \mathrm{Gain\_EM}}{(R_* \times t \times \mathrm{Gain\_EM} + R_{\mathrm{sky}} \times t \times n_{\mathrm{pix}} \times \mathrm{Gain\_EM})^{1/2} \times \sqrt{2}}. \tag{3}$$

The equation describing photometric accuracy is written as

$$\sigma(m) = \pm 2.5 \log\left(1 + \frac{1}{\mathrm{S/N}}\right). \tag{4}$$

Below is a legend of the symbols.

Symbol	Legend	Unit
R_*	count rate of star collected by detector	$\mathrm{e}^-\ \mathrm{s}^{-1}$
$R_{\rm sky}$	count rate of background collected by detector	$\mathrm{e}^-\ \mathrm{s}^{-1}\ \mathrm{pixel}^{-1}$
$R_{\rm obj}$	count rate from star	$\mathrm{e}^-\ \mathrm{s}^{-1}$
t	exposure time	s
$n_{\rm pix}$	number of pixels in aperture	–
D	dark current	$\mathrm{e}^-\ \mathrm{s}^{-1}\ \mathrm{pixel}^{-1}$
Gain	inverse-gain	$\mathrm{e}^-\ \mathrm{ADU}^{-1}$
Gain$_{\rm EM}$	EM gain of EMCCD	–
RN	readout noise	$\mathrm{e}^-\ \mathrm{pixel}^{-1}$
QE	quantum efficiency	–
k'	extinction coefficient	magnitude
$k' \times$ airmass	atmospheric extinction	magnitude

For a star of 10th magnitude in the V band of a Johnson/Bessel system, we compared the photometric accuracy of the three cameras with a 25 cm telescope and exposure time of 1 s when the airmass was around 1. Based on the conditions at Xinglong Observatory, we set $R_{\rm sky} = 20\,\mathrm{e}^-\ \mathrm{s}^{-1}\ \mathrm{pixel}^{-1}$, $k' = 0.201$ magnitude (Zheng et al. 2009), $n_{\rm pix}$ = 9 to match the pixel size of seeing (Warner 2006), and D = 0 to ignore dark current. Peak QEs are used during the calculation. For the EMCCD, we calculated the photometric accuracies for both cases where EM gain was turned off and was set at 4. The calculated photometric accuracies are shown in Table 4.

Table 4 The calculated results of the photometric accuracies[1] of a 10th magnitude star with a 25 cm telescope in the V band of the Johnson/Bessel system.

Camera	System Readout Rate	Preamp setting	Gain	RN	Photometric accuracy
sCMOS	280 MHz 16-bit	Dual	0.66	1.14	0.77%
FFCCD	2 MHz 16-bit	Low	4.17	7.33	0.59%
EMCCD	10 MHz 14-bit	2.4	21.13	50.29	0.76%[2] ; 0.42%[3]

Notes: [1] During the calculation, we set t: 1 s, $R_{\rm sky}$: $20\,\mathrm{e}^-\ \mathrm{s}^{-1}\ \mathrm{pixel}^{-1}$, k': 0.201 magnitude, $n_{\rm pix}$: 9, airmass: 1, D: 0, and QE: Peak QE (Table 1). [2] EM gain is turned off. [3] EM gain is set at 4.

3 EVALUATION

The sCMOS is used as the detector of the 25 cm telescope at Xinglong Observatory. The 1 m telescope is equipped with a 3-channel CCD photometer; each channel has an independent CCD camera and is controlled by the same computer (Mao et al. 2013). Both pieces of equipment use the filter system from the Sloan Digital Sky Survey (SDSS) (Fukugita et al. 1996).

The raw data are reduced by using the Image Reduction and Analysis Facility (IRAF).

3.1 Bias

To evaluate the stability of the cameras' bias, we acquired 100 bias frames for each camera under settings shown in Table 2, and calculated the mean values and the root mean square (RMS) of biases by using the imstatistics task in IRAF. The results (Table 5, Fig. 3) show that the sCMOS performs well in terms of bias correction thanks to its stable bias.

3.2 Gain and Readout Noise

In order to evaluate the gain, RN and to characterize their uniformity, we divide the image into nine sub-regions (Table 6). The gain and RN of each sub-region are calculated by using the findgain task in IRAF. The raw biases and flats were obtained under the settings shown in Table 2.

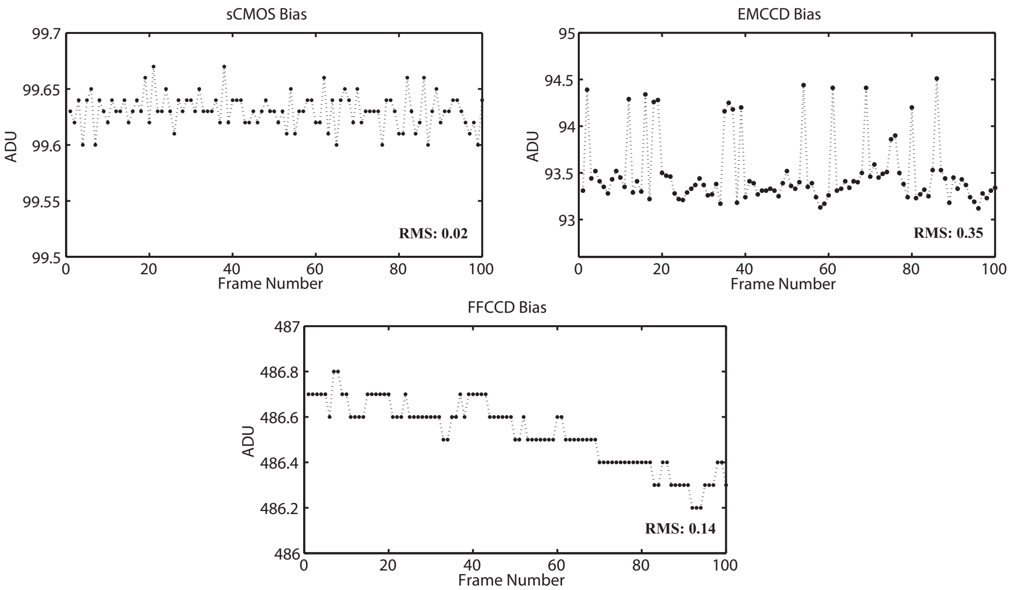

Fig. 3 The stabilities of 100 bias frames from the sCMOS, EMCCD, and FFCCD.

Table 5 The Mean Values and RMS of the Bias

Camera	Mean value	RMS
sCMOS	99.63	0.02
FFCCD	486.53	0.14
EMCCD	93.49	0.35

Table 6 The Position of Each Sub-region of the Image Acquired by the sCMOS, EMCCD and FFCCD

Camera	sCMOS		EMCCD		FFCCD	
Region	x	y	x	y	x	y
A	80:880	30:730	60:360	960:660	70:470	1250:850
B	880:1680	30:730	360:660	960:660	470:870	1250:850
C	1680:2480	30:730	660:960	960:660	870:1270	1250:850
D	80:880	730:1430	60:360	660:360	70:470	850:450
E	880:1680	730:1430	360:660	660:360	470:870	850:450
F	1680:2480	730:1430	660:960	660:360	870:1270	850:450
G	80:880	1430:2130	60:360	360:60	70:470	450:50
H	880:1680	1430:2130	360:660	360:60	470:870	450:50
I	1680:2480	1430:2130	660:960	360:60	870:1270	450:50

The gain and RN of each sub-region are shown in Figure 4. The specifications gain and RN of the sCMOS, EMCCD and FFCCD derived from the tests (Table 7) and those from the manufacturers (Table 2) are approximately equal. The stable gain and RN of the sCMOS ensure a high accuracy during data reduction.

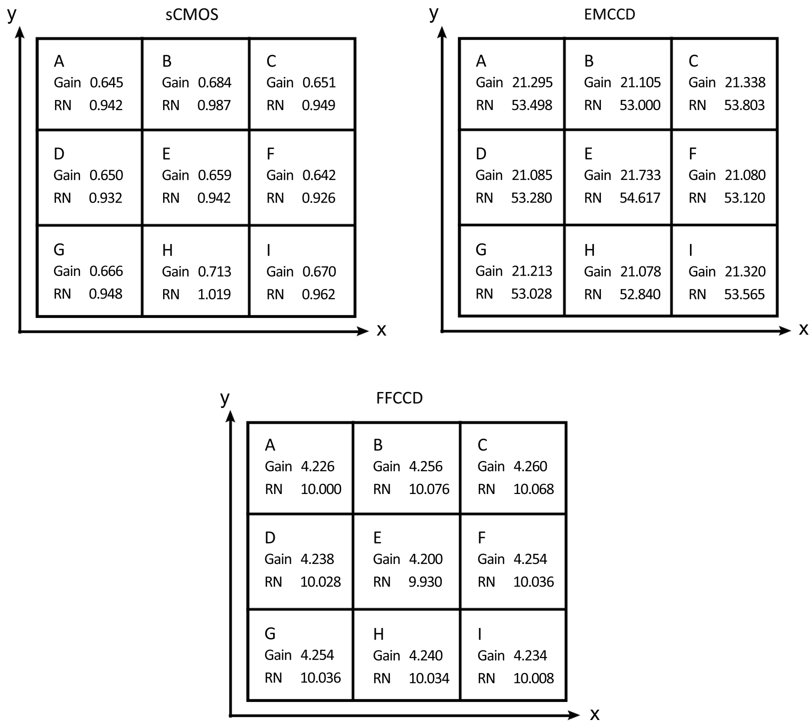

Fig. 4 The gain and RN of each sub-region of the sCMOS, EMCCD and FFCCD.

Table 7 The Gain, RN and RMS of the sCMOS, FFCCD and EMCCD

Camera	System Readout Rate	Preamp setting	Gain	RN	RMS (Gain)	RMS (RN)
sCMOS	280MHz 16-bit	Dual	0.66	0.96	0.022	0.029
FFCCD	2MHz 16-bit	Low	4.24	10.02	0.019	0.043
EMCCD	10MHz 14-bit	2.4	21.25	53.42	0.21	0.55

3.3 Linearity

In order to characterize the linearity of these cameras, we acquired a series of images with increasing exposure time until the images reached saturation. The combined bias was subtracted from all images, and signals from the central 100×100 pixels were averaged. The settings were fixed as shown in Table 2.

The results show that the linearity of the sCMOS, EMCCD and FFCCD is about 99.9% up to 29 400 e^-, 99.7% up to 83 900 e^-, and 99.8% up to 205 000 e^-, respectively (Fig. 5).

3.4 Pixel Nonuniformity

Pixel nonuniformity is the variation in pixel sensitivity with respect to incident photons (Janesick 2001). The conventional CMOS cameras have higher pixel nonuniformity when compared with CCD cameras, due to their differing pixel structures. All pixels of a CCD camera share the same output amplifier at the end of the chip, but each pixel of a CMOS camera has its own output circuits. The

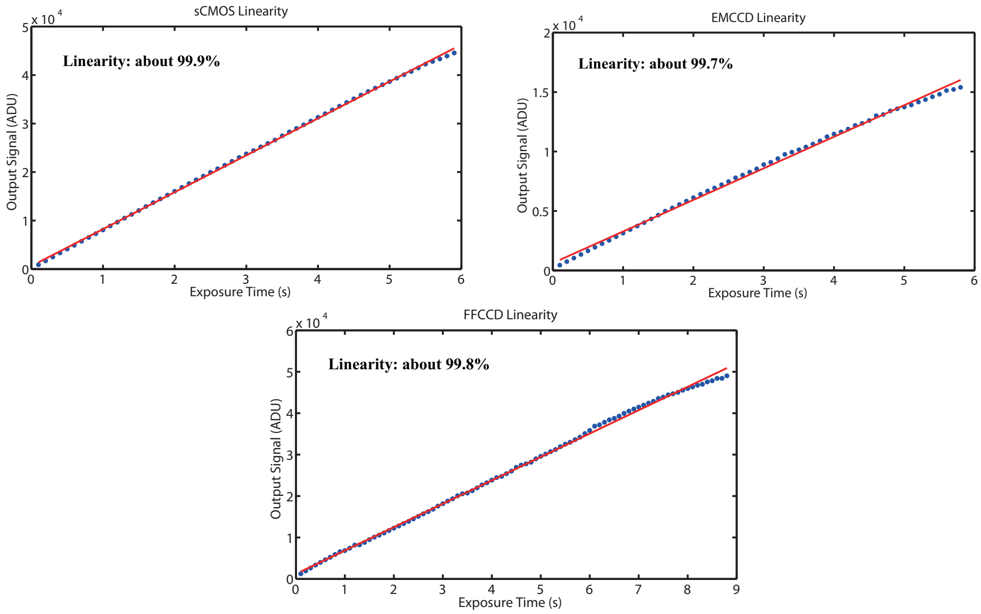

Fig. 5 Linear response curve of the sCMOS, EMCCD and FFCCD.

pixel nonuniformity in cameras can be evaluated using flat images, which is described as follows

$$P_N = \frac{\sigma_A}{\overline{A}}, \tag{5}$$

where σ_A is RMS of flat image pixels and $\overline{A}$ is the mean value of flat image pixels (Janesick 2007, Shang & Song 2006).

We obtained dome flats (about half saturation) and subtracted their combined bias. A region of the central 100×100 pixels is used to evaluate the pixel nonuniformity. The value of each pixel in the region is shown in Figure 6. The pixel nonuniformity of the sCMOS, EMCCD and FFCCD is approximately 0.95%, 0.81% and 0.52%, respectively.

3.5 Photometric Accuracy

We observed the SDSS standard star Hilt 566 (Table B.1) using the 25 cm telescope equipped with the sCMOS on 2011 December 25. The same standard star was observed using the 1m telescope equipped with the FFCCD and EMCCD[2] on 2011 November 9. The weather conditions were stable and clear during the observations. The raw images are shown in Figure 7. The field of view (FOV) of images is different due to different focal lengths and different chip sizes.

The SDSS standard star Hilt 566 was observed when it was close to meridian transit. For a comparison of the three cameras, the data obtained by the 1m telescope were transformed into a representation describing the 25 cm telescope system by considering the differences of apertures and efficiencies of the two systems. The exposure time was reduced to 1 s. The relationships between the magnitudes and photometric accuracies of stars in this field are shown in Figure 8, where values greater than three sigma are removed. The photometric accuracy of the sCMOS is approximately equal to that of the EMCCD and FFCCD in both i' and r' bands (Table 8). Due to the influence

[2] EM gain was set to 4 during the observations with consideration of the well depth of the active area of the pixel and the well depth of gain register of the pixel.

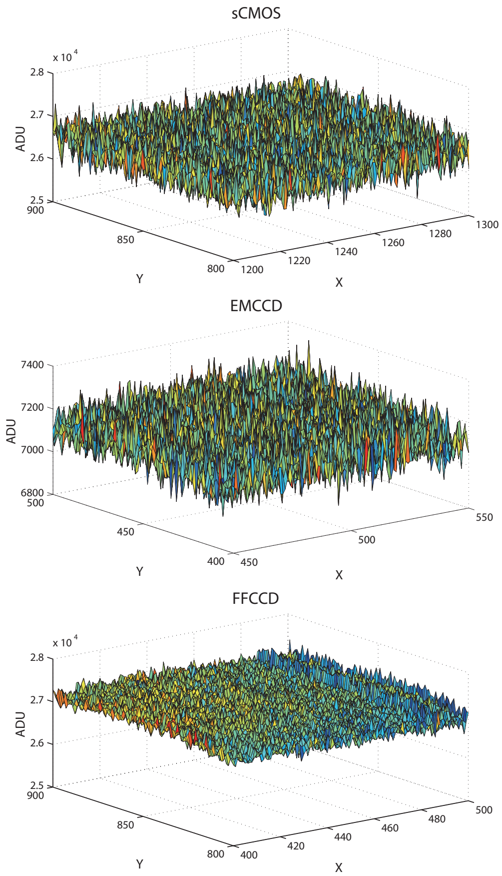

Fig. 6 The graph of surface flats of the sCMOS, EMCCD and FFCCD. The pixel nonuniformity of the sCMOS, EMCCD and FFCCD is approximately 0.95%, 0.81%, 0.52%, respectively.

of the telescope systems' efficiencies, different filter systems and weather conditions, the observed results of the photometric accuracies are worse than those from the calculations (Table 4).

3.6 Photometric Stability

In order to evaluate the photometric stability of the three cameras, the sCMOS, EMCCD and FFCCD were equipped on the 25 cm telescope to observe the SDSS standard stars under photometric conditions. We characterized the photometric stability of these cameras by using the variation of the differential magnitude of the two standard stars in the same FOV. For the sCMOS and EMCCD, we observed 30 frames of the SDSS standard stars SA108–475 and SA108–551 (Table B.1) in the same FOV in the SDSS r' band with 20 s and 10 s exposure times, respectively. The RMS of the differential magnitude of the sCMOS and EMCCD between SA108–475 and SA108–551 is 0.0085 and 0.0094, respectively. For FFCCD, we also observed 30 frames of the SDSS standard stars SA113–466 and SA113–475 (Table B.1) in the same FOV in the SDSS r' band with a 13 s exposure time. The RMS of the differential magnitude of the FFCCD between SA113–466 and SA113–475 is 0.0089 (Fig. 9).

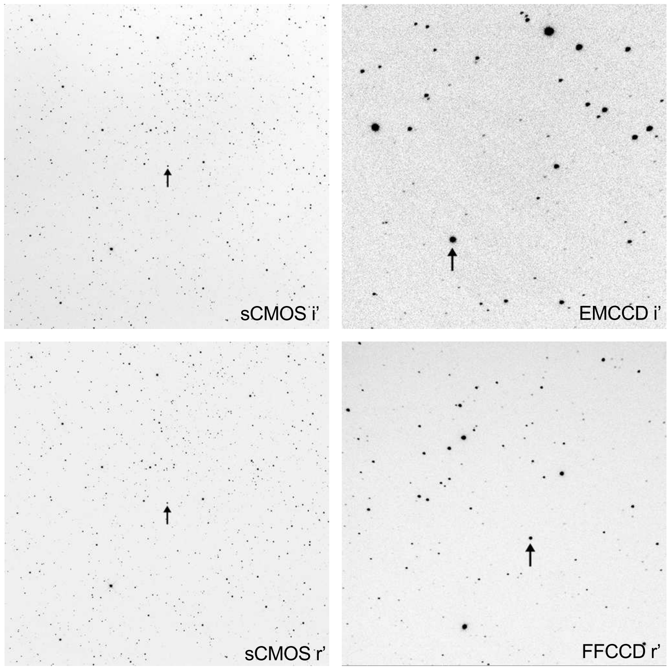

Fig. 7 The raw data of Hilt 566 taken by the sCMOS, EMCCD and FFCCD. The FOV of the sCMOS, FFCCD and EMCCD is $1.06^\circ\ \times 0.89^\circ$, 18.42$'$ $\times$ 17.87$'$ and $9.14' \times 9.14'$, respectively.

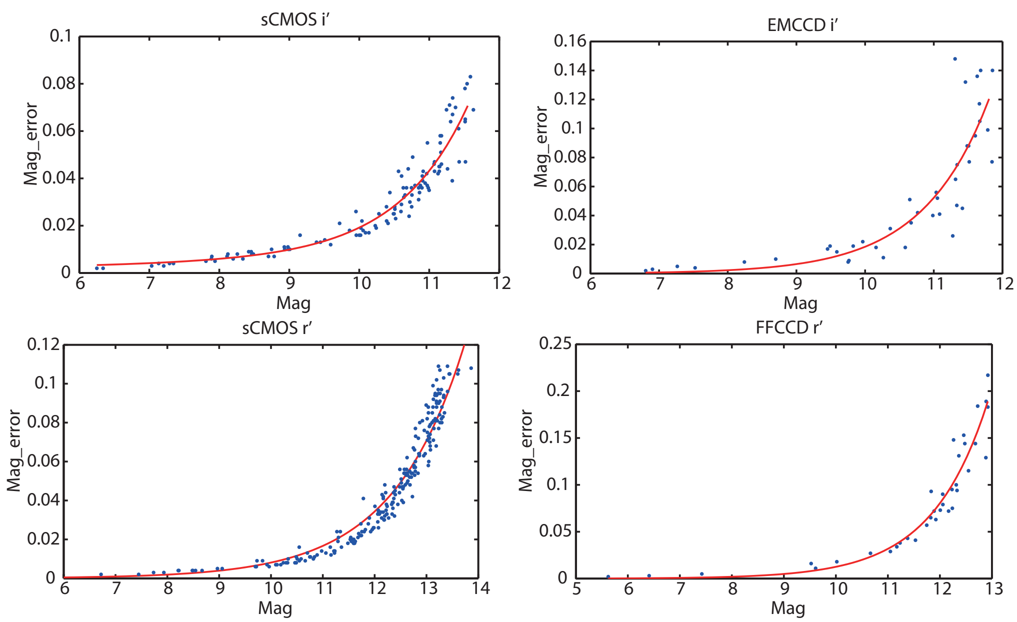

Fig. 8 The magnitudes and photometric accuracies of stars observed by the sCMOS, EMCCD and FFCCD in the i' and r' bands.

Table 8 The photometric accuracies of different magnitudes in the i' and r' bands. The data were transformed into a representation describing the 25 cm telescope system and 1 s exposure time.

	Mag	Mag_error		Mag	Mag_error
sCMOS i'	7	0.3%	EMCCD i'	7	0.3%
	8	0.5%		8	0.4%
	9	1.0%		9	0.7%
	10	2.0%		10	1.5%
	11	4.3%		11	3.8%
	Mag	Mag_error		Mag	Mag_error
sCMOS r'	7	0.1%	FFCCD r'	7	0.1%
	8	0.2%		8	0.2%
	9	0.4%		9	0.5%
	10	0.8%		10	1.3%
	11	1.7%		11	3.2%

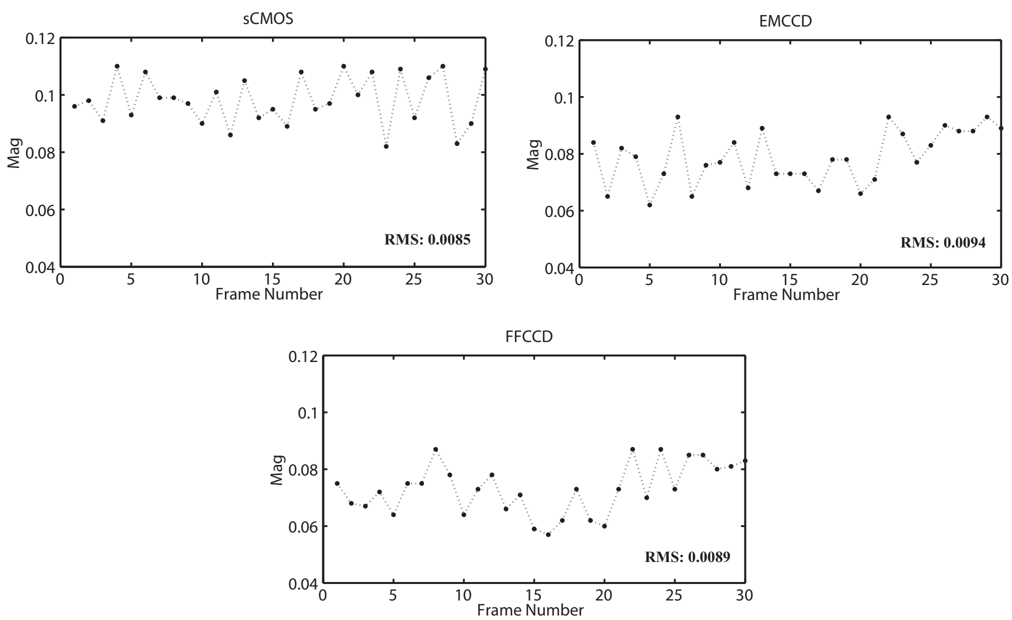

Fig. 9 The differential magnitude curve of 30 frames in the SDSS r' band for the sCMOS, EMCCD and FFCCD.

4 CONCLUSIONS

In this paper, by comparing with the FFCCD and EMCCD, we evaluate the bias, gain, RN, linearity, pixel nonuniformity, dynamic range, photometric accuracy and stability of the sCMOS.

The results show that the sCMOS has a good linearity (about 99.9%) up to 29 400 e^- at the setting of 280 MHz 16-bit Dual –40°C and a high frame rate with low RN. The pixel-to-pixel nonuniformity is less than 1%. The bias and photometric performance are stable in the tests. The evaluations show that the sCMOS could give similar performances as the FFCCD and EMCCD we tested, except for QE and fill factor. According to the results of the observations, the photometric accuracies of the sCMOS are approximately equal to those of the FFCCD and EMCCD. It seems that the photometric accuracies are little affected by the fill factor of the sCMOS. Therefore, we need more data from observations of both oversampling and undersampling to analyze the relationship between fill factor and photometric accuracy. Because of the lower QE, the sCMOS is not a good choice for faint sources due to more exposure time being required. However, it could be used to observe bright sources, particularly when high spatial or temporal resolution is desired.

Consequently, the sCMOS can be very useful for some astronomical observations thanks to its unique properties. It can be used in lucky imaging which requires a high frame rate to avoid the influence of seeing. It also meets the requirements of solar observation in studies of solar granulation and activities, because of the small pixels, high dynamic range and high frame rate with low RN. Moreover, it can be applied in offset guiding due to high temporal resolution, stable operation and portable size.

Acknowledgements We thank Jianfeng Wang and Jin Ma for their kind support in evaluating the performance of the sCMOS. We thank Dawei Xu, Huijuan Wang, Liang Ge, Xuezheng Su and Qin Lin for helpful discussions. We acknowledge Wan Zhou, Jiupeng Guo and Fengfeng Mi for their long-term help during observing runs.

Appendix A: SPECIFICATIONS OF THE SCMOS, FFCCD AND EMCCD

Table A.1 Detailed Specifications of the sCMOS in Rolling Shutter Readout Mode[1]

System Readout Rate	Preamp setting	Gain	Readout Noise
280 MHz	PAG1	17.82	11.27
	PAG2	8.73	5.66
	PAG3	1.77	1.96
	PAG4	0.66	1.14
	Dual (PAG1 and PAG4)	0.66	1.14
200 MHz	PAG1	18.29	10.66
	PAG2	8.91	5.71
	PAG3	1.73	1.83
	PAG4	0.63	0.97
	Dual (PAG1 and PAG4)	0.63	0.97
100 MHz	PAG1	19.41	11.81
	PAG2	9.27	6.08
	PAG3	1.74	1.70
	PAG4	0.60	0.84
	Dual (PAG1 and PAG4)	0.60	0.84

Notes: [1] The specifications of the sCMOS are from the manufacturer, Andor Technology. The specifications RN and Gain of Dual are typically the same as that of PAG4.

Table A.2 Detailed Specifications of the EMCCD[1]

System Readout Rate	Preamp setting	Gain	Readout Noise
10 MHz 14-bit EM amplifier	1	–	–
	2.4	21.13	50.29
	5	10.00	45.00
5 MHz 14-bit EM amplifier	1	48.00	73.44
	2.4	19.01	44.86
	5	8.58	35.95
3 MHz 14-bit EM amplifier	1	46.98	54.50
	2.4	18.64	31.69
	5	8.48	26.03
1MHz 16-bit EM amplifier	1	18.43	32.25
	2.4	7.26	20.18
	5	3.32	17.20
3 MHz 14-bit CON amplifier	1	9.97	14.06
	2.4	4.02	10.65
	5	1.81	9.83
1 MHz 16-bit CON amplifier	1	3.75	8.25
	2.4	1.53	6.75
	5	0.68	6.21

Notes: [1] The specifications of the EMCCD are from the manufacturer, Andor Technology.

Table A.3 Detailed Specifications of the FFCCD[1]

System Readout Rate 16bit	Preamp setting	Gain	Readout Noise
100 kHz	High	1.15	3.62
	Mid	2.25	
	Low	4.47	
2 MHz	High	1.04	7.33
	Mid	2.08	
	Low	4.17	

Notes: [1] The specifications of the FFCCD are from the manufacturer, Princeton Instruments.

Appendix B: THE SDSS STANDARD STARS

Table B.1 The SDSS Standard Stars which were Used during Observations

Star Name	RA (J2000.0)	Dec (J2000.0)	r'	$u'-g'$	$g'-r'$	$r'-i'$	$i'-z'$
Hilt 566	06:32:09.67	+03:34:44.4	10.787	1.125	0.673	0.341	0.211
SA 108 475	16:37:00.60	–00:34:39.0	10.832	3.127	1.130	0.456	0.270
SA 108 551	16:37:47.79	–00:33:05.1	10.747	1.256	–0.032	–0.104	–0.051
SA 113 466	21:41:27.39	+00:40:15.6	9.908	1.125	0.275	0.073	–0.005
SA 113 475	21:41:51.30	+00:39:20.8	9.979	2.255	0.817	0.318	0.166

References

Andor Technology Low-light Imaging Cameras, *iXon*$^{\mathrm{EM}}$ +888 (back-illuminated), 2009 (*http://www.andor.com/ scientific_cameras/ixon/*)

Andor Technology Neo sCMOS Camera, sCMOS DC-152Q-FI, 2010 (*http://www.andor.com/scientific_cameras/neo_scmos_camera/*)

Andor Technology, Andor Technology NEO sCMOS Technical Notes, 2010 (*http://www.andor.com/ scientific-cameras/ neo-and-zyla-scmos-cameras/neo-scmos*)

Andor Technology, Unravelling Sensitivity, Signal to Noise and Dynamic Range – EMCCD vs CCD, 2009 (*http://www.emccd.com/what_is_emccd/unraveling_sensitivity/*)

Fukugita, M., Ichikawa, T., Gunn, J. E., et al. 1996, AJ, 111, 1748

Hoffman, A., Loose, M., & Suntharalingam, V. 2005, Experimental Astronomy, 19, 111

Howell, S. B. 2006, Handbook of CCD Astronomy (2nd ed.; Cambridge University Press)

Janesick, J., Gunawan, F., Dosluoglu, T., Tower, J., & McCaffrey, N. 2002, Experimental Astronomy, 14, 33

Janesick, J. R. 2001, Scientific Charge-Coupled Devices (Bellingham: SPIE Press)

Janesick, J. R. 2007, Photon Transfer DN $\rightarrow \lambda$, ed. James R. Janesick (Bellingham: SPIE Press)

Mao, Yong-Na, Lu, Xiao-Meng, Wang, Jian-Feng, & Xiao-Jun Jiang 2013, RAA (Research in Astronomy and Astrophysics), 13, 239

Princeton Instruments, PIXIS: 1300B, Standard System Data Sheet, 2005 (*http://www.princetoninstruments.com/products/imcam/pixis/*)

Shang, Y., & Song, Q. 2006, in Society of Photo-Optical Instrumentation Engineers (SPIE) Conference Series, 6276, 436

Waltham, N. 2010, ISSI Scientific Reports Series, 9, 391

Warner, B. D. 2006, A Practical Guide to Lightcurve Photometry and Analysis (Berlin: Springer Verlag)

Zheng, W.-K., Qiu, Y.-L., Wang, J., et al. 2009, Publications of the National Astronomical Observatories of China, 6, 136